Journal of Controlled Release 357 (2023) 630–640

Contents lists available at ScienceDirect

Journal of Controlled Release

journal homepage: www.elsevier.com/locate/jconrel

Surface display of functional moieties on extracellular vesicles using lipid anchors

Wenyi Zheng [a,c,*], Melanie Schürz [b], Rim Jawad Wiklander [a,c], Oskar Gustafsson [a,c], Dhanu Gupta [a,c], Radka Slovak [d], Andrei Traista [d], Arianna Coluzzi [d], Samantha Roudi [a,c], Antonella Barone [e], Daria Farcas [d], Eleni Kyriakopoulou [d], Valentina Galli [d], Heena Sharma [d], Nicole Meisner-Kober [b], Malgorzata Honcharenko [a,c,d,*], Samir E.L. Andaloussi [a,c,d,*]

[a] Biomolecular Medicine, Division of Biomolecular and Cellular Medicine, Department of Laboratory Medicine, Karolinska Institutet, Huddinge, Sweden
[b] Department of Biosciences and Medical Biology, Paris Lodron University Salzburg, Salzburg, Austria
[c] Centre for Allogeneic Stem Cell Transplantation, Karolinska University Hospital, Huddinge, Sweden
[d] EVOX Therapeutics Limited, Oxford, United Kingdom
[e] Department of Experimental and Clinical Medicine, The Magna Græcia University of Catanzaro, Catanzaro, Italy

ARTICLE INFO

Keywords:
Lipophilic dye
Dissociation
Exosome
Uptake
Targeting
Half-life

ABSTRACT

Extracellular vesicles (EVs) are efficient natural vehicles for intercellular communication and are under extensive investigation for the delivery of diverse therapeutics including small molecule drugs, nucleic acids, and proteins. To understand the mechanisms behind the biological activities of EVs and develop EV therapeutics, it's fundamental to track EVs and engineer EVs in a customized manner. In this study, we identified, using single-vesicle flow cytometry and microscopy, the lipid DOPE (dioleoyl phosphatidyl ethanolamine) as an efficient anchor for isolated EVs. Notably, DOPE associated with EVs quickly, and the products remained stable under several challenging conditions. Moreover, conjugating fluorophores, receptor-targeting peptides or albumin-binding molecules with DOPE enabled tracking the cellular uptake, enhanceing the cellular uptake or extending the circulation time in mice of engineered EVs , respectively. Taken together, this study reports an efficient lipid anchor for exogenous engineering of EVs and further showcases its versatility for the functionalization of EVs.

1. Introduction

Extracellular vesicles (EVs) are natural particles secreted by cells and implicated in a wide range of physiological and pathological contexts. Besides horizontal transfer of cargo molecules like proteins and RNAs between cells, EVs can induce signaling in target cells upon interaction at cell surface (juxtacrine signaling) [1] as well as complex with and neutralize soluble factors through natural or synthetic receptors on EV surface (decoy effect) [2]. Moreover, EVs have intrinsic tropism at the tissue and cell levels as a result of the surface molecules. The various functions in combination with favorable safety profiles of EVs are inspiring accumulating efforts to develop EV-based therapeutics [3].

To understand the mechanisms behind the biological activities of EVs and develop EV therapeutics, it's fundamental to track EVs specifically and engineer EVs in a customized manner. Endogenous engineering of EV producer cells is a common way to label and functionalize EVs [4–6]. Despite its high specificity and robustness, there exist many situations precluding genetic engineering, especially upon studying EVs of unspecified cellular sources. In contrast, exogenous engineering of pre-isolated EVs bypasses the requirement of manipulating EV source cells and can be adapted for various kinds of applications. Functional moieties can be stably coupled with amines on EV surface, but this method requires lengthy reaction and purification steps [4,7]. In addition, external forces from sonication and electroporation have been utilized to engineer EVs, while the processes are limited by low engineering efficiency as well as concerns about the integrity of EVs and payloads [8]. Alternatively, physical association between functional moieties and EVs is often applied as a result of its simpler procedure.

Lipids with fluorescent tags are widely used for cellular staining due to their high affinity to plasma membrane. The lipid bilayer of EVs

* Corresponding authors at: Biomolecular Medicine, Division of Biomolecular and Cellular Medicine, Department of Laboratory Medicine, Karolinska Institutet, Huddinge, Sweden.
E-mail addresses: wenyi.zheng@ki.se (W. Zheng), malgorzata.honcharenko@ki.se (M. Honcharenko), samir.el-andaloussi@ki.se (S.E.L. Andaloussi).

https://doi.org/10.1016/j.jconrel.2023.04.033
Received 16 January 2023; Received in revised form 28 February 2023; Accepted 18 April 2023
Available online 24 April 2023

renders them with strong potential for the anchorage of lipid conjugates. Indeed, cholesterol, ceramides, and phosphatidylethanolamines are reportedly used as lipid anchors for attaching functional moieties onto EVs [9–12]. However, the relative engineering efficiency of those lipids remains unknown, mainly due to the lack of an informative method enabling head-to-head comparison. As such, this study aims to compare the engineering efficiency of reported lipid anchors and identify a robust alternative for exogenous engineering of EVs.

Noteworthy, DOPE stood out as the most efficient anchor for EV engineering among the seven candidates, including the benchmark cholesterol. Moreover, after conjugation with different functional moieties, DOPE-based engineering enabled reliable tracking of cellular uptake, increased cellular uptake and extended retention in mouse plasma of engineered EVs.

2. Results

2.1. DOPE outperforms ceramide and cholesterol in engineering EVs

Exogenous engineering of EVs by means of physical association is limited by the lack of an efficient lipid anchor. In search of an ideal anchor, EVs were collected from two model producer cell lines, FreeStyle 293-F and K562, to gain insight into the influence of EV origins on engineering efficiency (Fig. S1a, Fig. S1b). Cholesterol, a widely reported lipid anchor for exogenous engineering of EVs [9,10], was the benchmark in our study. In addition, some studies have used fluorescent conjugates of ceramide [13] and DOPE (dioleoyl phosphatidylethanolamine) for labeling EVs [14], but their relative efficiency to cholesterol has not been studied (Fig. 1a). To fill in the gap, the three lipids were tagged with the fluorophore NBD (Fig. S1c) and incubated with EVs at the same dye:EV ratio. Without further purification procedures, EV-lipid mixture was analyzed for the concentration and mean fluorescence intensity (MFI) of NBD-positive events using single-vesicle image-based flow cytometry (Fig. 1b, Fig. S1d) [15]. Lipids were incubated with PBS

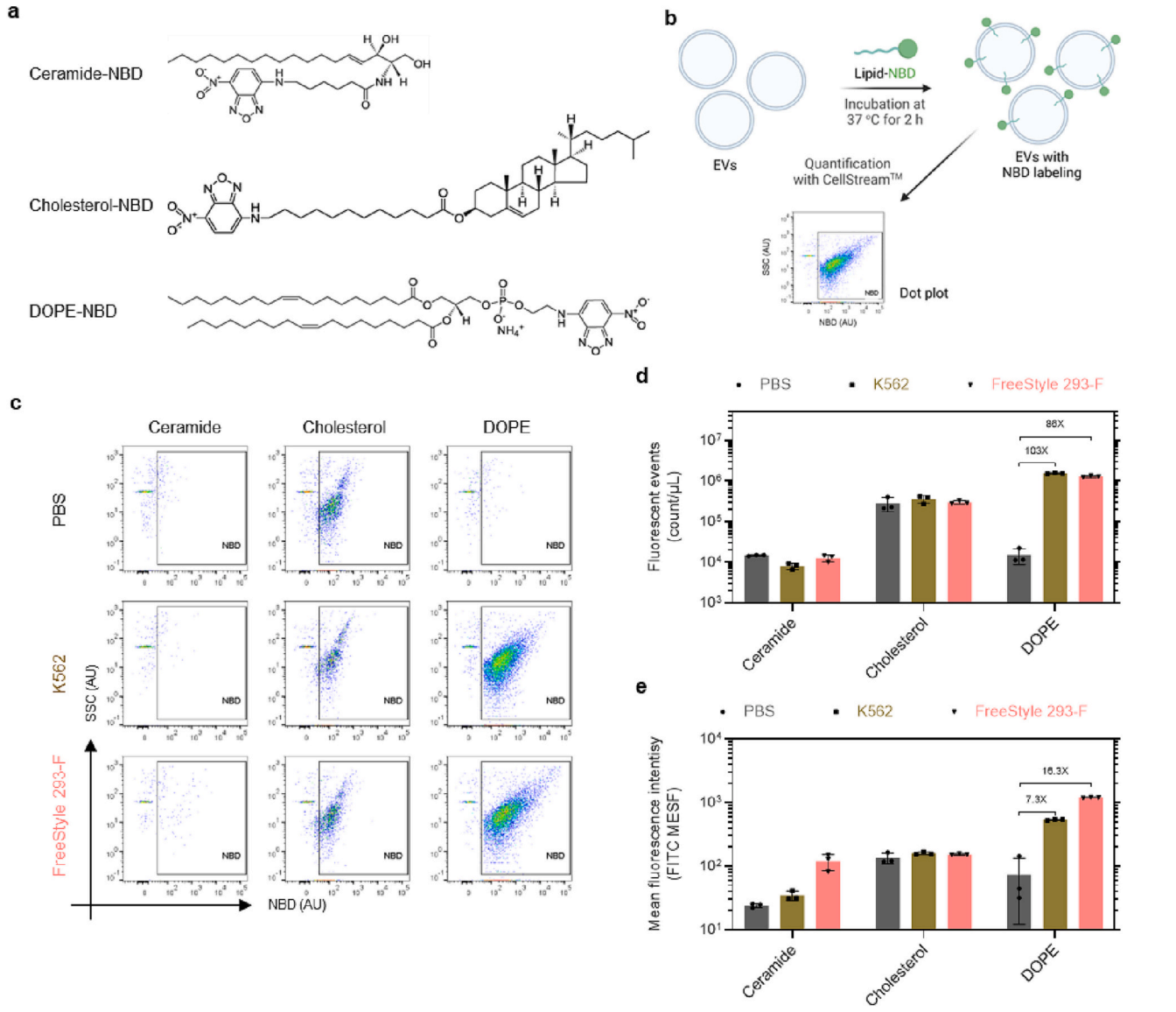

Fig. 1. EV engineering efficiency of ceramide, cholesterol, and DOPE. (a) Chemical structure of NBD-tagged lipids. (b) Scheme of labeling and detection of EVs. EVs were incubated with NBD-tagged lipid conjugates (3e5 molecules per EV) for 2 h at 37° C and analyzed by CellStream. (c) Representative dot plot of engineered EVs. (d) Concentration of NBD-positive events. (e) Mean fluorescence intensity of NBD-positive events. In (d-e), data were shown as the mean ± standard deviation of three biological replicates.

to account for background signals resulting from potential dye aggregation.

Surprisingly, ceramide failed to label any EVs, and cholesterol induced noticeable aggregation precluding specific detection of labeled EVs (Fig. 1c). In contrast, DOPE had high engineering efficiency for EVs from FreeStyle 293-F and K562 cells without significant dye aggregation. Subsequent quantification confirmed substantial increases in the concentration (> 86-fold; Fig. 1d) as well as MFI (> 7.3-fold; Fig. 1e) of NBD-positive events relative to the background. Overall, our results identify DOPE as a superior anchor to ceramide and cholesterol for EV engineering.

2.2. DOPE outperforms its analogs in engineering EVs

In recent publications, another type of phosphatidylethanolamine with distearoyl chains (*i.e.*, DSPE) was used as the lipid anchor for EV engineering [16–18]. To understand the importance of fatty acid chain, we selected a few phosphatidylethanolamine lipids with different fatty acid and examined their relative engineering efficiency using the same protocol as above. Those lipids were all tagged with NBD (Fig. 2a). Interestingly, the loss of one oleoyl chain in DOPE (*i.e.*, Lyso-DOPE) almost completely abolished the EV engineering ability, with only a few NBD-positive EVs detected (Fig. 2b), underlying the critical role of both oleoyl chains. In addition, changing oleoyl to palmitoyl (*i.e.*, DPPE) or stearoyl (*i.e.*, DSPE) decreased the concentration of NBD-positive EVs by >57% and 85%, respectively, compared to DOPE (Fig. 2c). Adding four methyl groups in the palmitoyl chain (*i.e.*, DPhPE) further reduced the engineering efficiency and induced significant self-aggregation with signal/background ratios <4.2-fold (Fig. S2). Moreover, results regarding MFI of engineered EVs suggest that DOPE-based engineering displayed more lipid conjugates per vesicle than its analogs (Fig. 2d). These data further confirm the excellent ability of DOPE in engineering EVs, most likely benefiting from the oleoyl chains.

2.3. DOPE robustly associates with EVs at different incubation conditions

Results above identified DOPE as a promising lipid anchor for EV engineering. To advance the engineering efficiency, the protocol employed above was adjusted in terms of DOPE concentration, as well as incubation temperature and duration. Among the concentration range tested (DOPE molecules per EV from 6e4 to 1.2e6), higher DOPE concentration resulted in a linear increase in background signals, whereas both the concentration and fluorescence intensity of engineered particles plateaued when the DOPE/EV ratio exceeded 3e5 (Fig. 3a-c). Data from another flow cytometer, NanoFCM, that can distinguish engineered EVs from lipid aggregates on basis of fluorescence intensity per particle well reconciled with that from CellStream (Fig. S3a-b). Specifically, both types of measurement show that DOPE-based engineering plateaued at the concentration of 3e5 DOPE molecules per EV irrespective of EV origin. Moreover, increasing DOPE concentrations above 1.2e6 per EV resulted in significant decreases in the percentage of NBD-positive EVs due to a greater occurrence of lipid aggregates.

Next, we examined different combinations of incubation temperature and duration to address future demands involving temperature-sensitive payloads and limited time. It appears that EVs had different degrees of reliance on incubation conditions depending on the origins (Fig. S3c). Regarding the concentration of engineered particles, EVs from FreeStyle 293-F cells were best engineered at relatively high

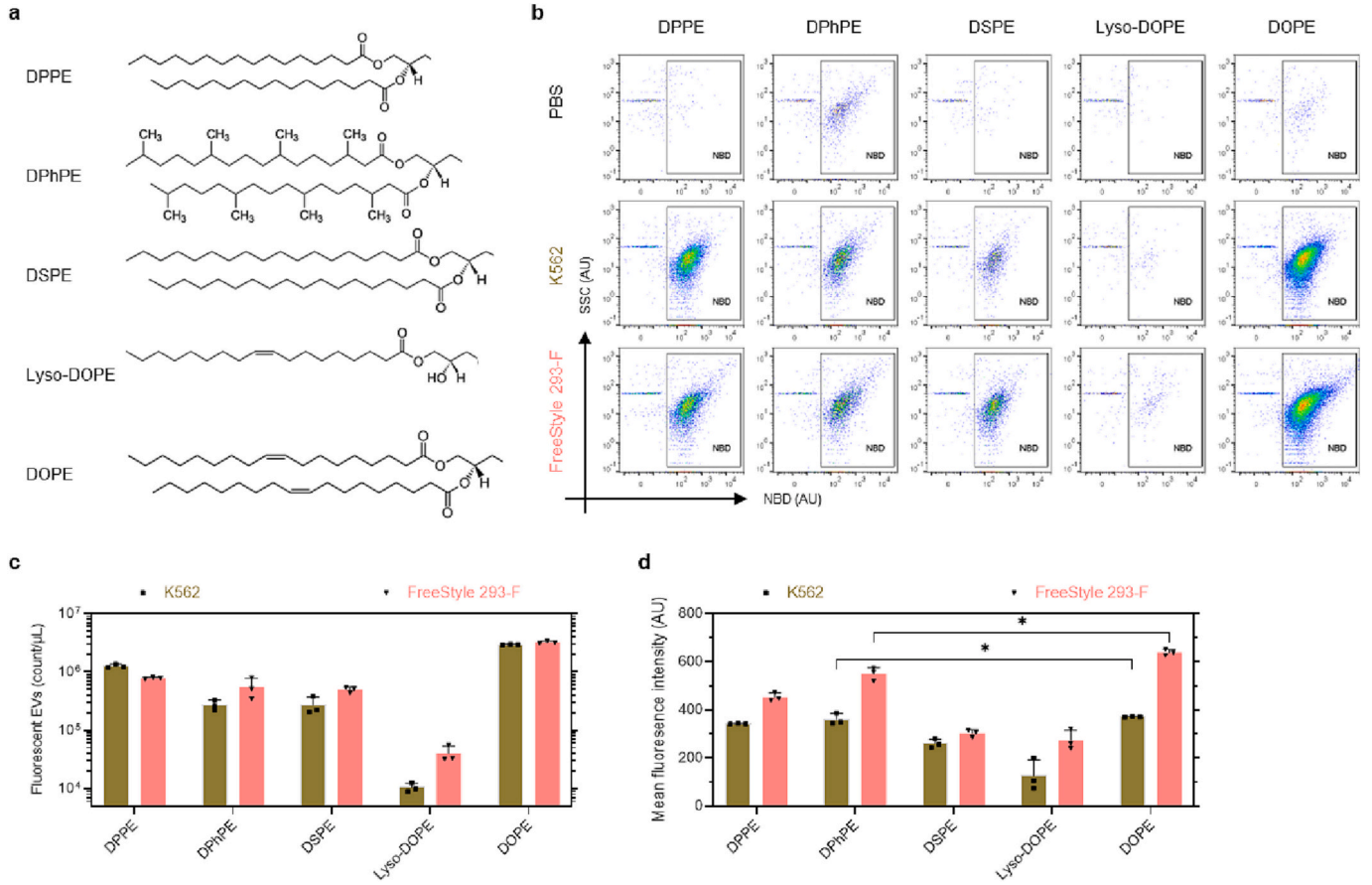

Fig. 2. EV engineering efficiency with DOPE analogs. (a) Chemical structure of DOPE analogs. (b) Representative dot plot of engineered EVs. EVs were incubated with NBD-tagged lipid conjugates (3e5 molecules per EV) for 2 h at 37°C. (c) Concentration of NBD-positive events. (e) Mean fluorescence intensity of NBD-positive events. In (c-d), data were shown as the mean ± standard deviation of three biological replicates. Two-tailed unpaired *t*-test. *: $p < 0.05$.

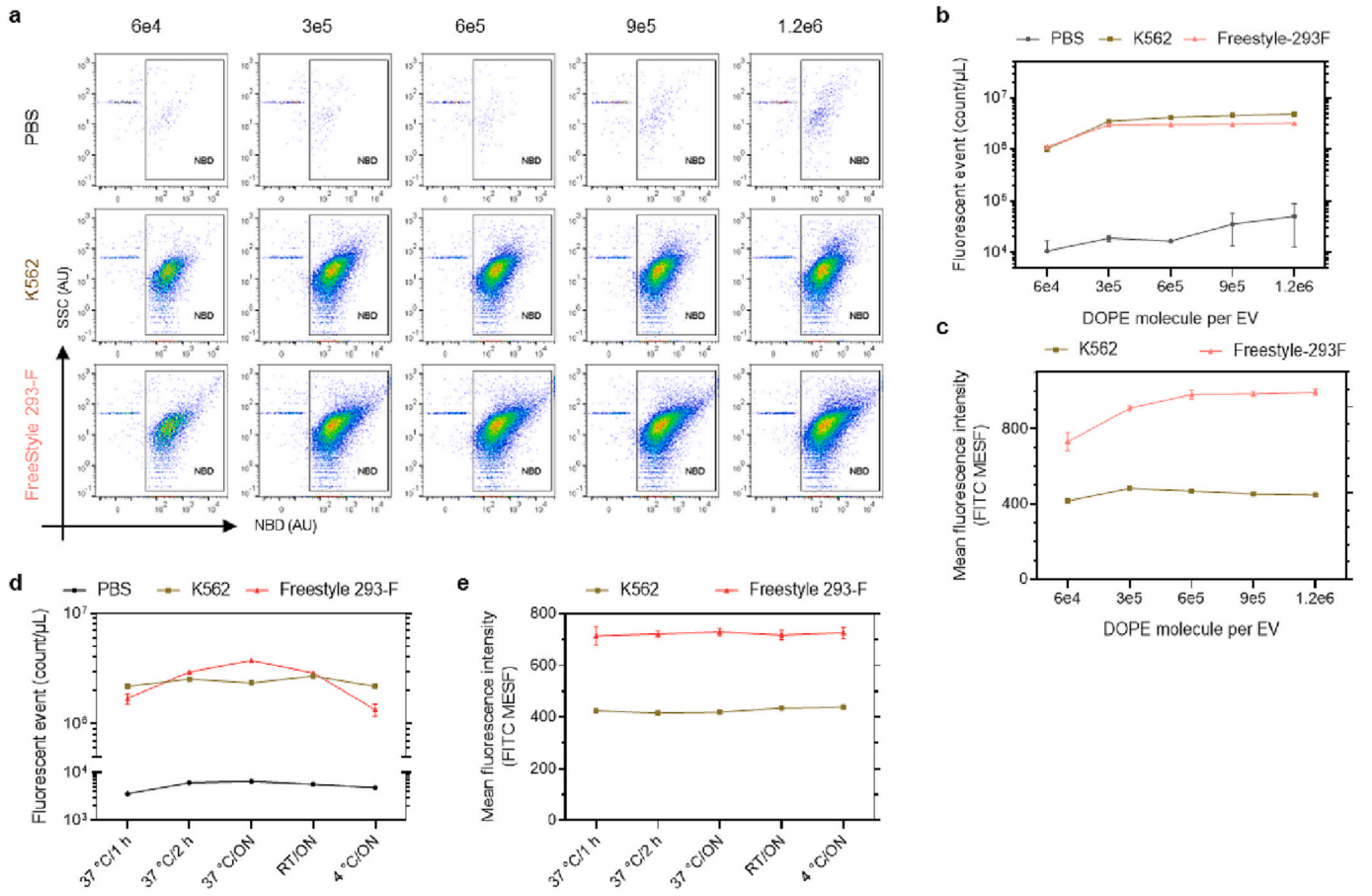

Fig. 3. EV engineering efficiency with DOPE at different conditions. (a) Representative dot plot of engineered EVs. EVs were incubated with different concentrations of DOPE-NBD conjugates for 2 h at 37° C. (b) Concentration of NBD-positive events at different labeling concentrations. (c) Mean fluorescence intensity of NBD-positive events at different labeling concentrations. (d) Concentration of NBD-positive events at different incubation conditions. (e) Mean fluorescence intensity of NBD-positive events at different incubation conditions. In (d-e), EVs were incubated with DOPE-NBD at a concentration of 3e5 molecules per EV. In (b-e), data were shown as the mean ± standard deviation of three biological replicates.

temperatures and long duration (37° C overnight), while K562-derived EVs were equally engineered under all tested conditions (Fig. 3d). The fluorescence intensity of engineered EVs was almost unaltered at different incubation conditions (Fig. 3e). Irrespective of the incubation conditions, K562-derived EVs always displayed fewer DOPE conjugates per EV than those from FreeStyle 293-F, probably due to their distinct membrane compositions and affinity to DOPE. After staining FreeStyle 293-F cells-derived EVs with DOPE-NBD (3e4 molecule per EV, 37° C for 2 h) and purification through size exclusion chromatography, the number of DOPE-NBD molecules per EV were calculated to approximate 24,701 (s.d. ± 850, $N = 3$). Taken together, DOPE-based engineering plateaus at a concentration of around 3e5 molecules per EV and can be robustly used independently of incubation conditions.

2.4. DOPE is compatible with other methods for labeling EVs

Next, we characterized the relative engineering efficiency of DOPE to other reported methods. Genetic engineering of EV producer cells offers high specificity in labeling EV subpopulations. Herein, EVs were isolated from FreeStyle 293-F cells stably expressing mNeonGreen (mNG) protein fused to a classic EV scaffold protein CD63, termed as CD63-mNG EVs, labeled with DOPE-NBD and purified. Analysis of the products by NTA did not show significant changes in size distribution (Fig. 4a). Electron microscopy images also indicate the typical membranous structure after engineering EVs with DOPE conjugates (Fig. 4b). To invesitigate the localization of DOPE, it was conjugated in-house with a far-red fluorescent molecule Cy5 (Fig. S4a) before incubation with EVs (Fig. 4c). Images from super-resolution fluorescence microscopy reveal spatial proximity between DOPE and CD63 molecules (Fig. 4d). Afterwards, the relative engineering efficiency was quantified using flow cytometry. All genetically engineered EVs became positive for Cy5, which confirms the prominent engineering efficiency of DOPE (Fig. 4e). Moreover, DOPE-based engineering led to greater yields than genetic engineering with around 60% of $Cy5^+$ EVs being negative in the mNG channel. A similar trend was observed while using single vesicle fluorescence microscopy (Fig. 4f) [19]. This might be attributable to the presence of $CD63\text{-}mNG^-$ particles in the EV preparation and/or infereior brightness of mNG to Cy5.

In addition to genetic engineering, chemical labeling is commonly used to track EVs *in vitro* and *in vivo*. For comparison of chemical labeling with DOPE, we used milk EVs that were pre-labeled with Cy7 NHS ester [20] and incubated them with DOPE-Cy5. Again, milk EVs were readily stained with DOPE-Cy5 (Fig. S4b). Overall, our results indicate that DOPE-based engineering is orthogonal to genetic and chemical engineering of EVs.

2.5. DOPE strongly associates with EVs

The fact that many hydrophobic dyes like DIR are susceptible to dissociation motivates us to characterize the stability of DOPE-engineered EVs. To this end, DOPE-engineered EVs were first purified and subjected to either a freeze/thaw cycle, incubation in Opti-MEM cell culture medium, or incubation in mouse serum. In analytical size exclusion chromatography, EVs are eluted at a specific retention time

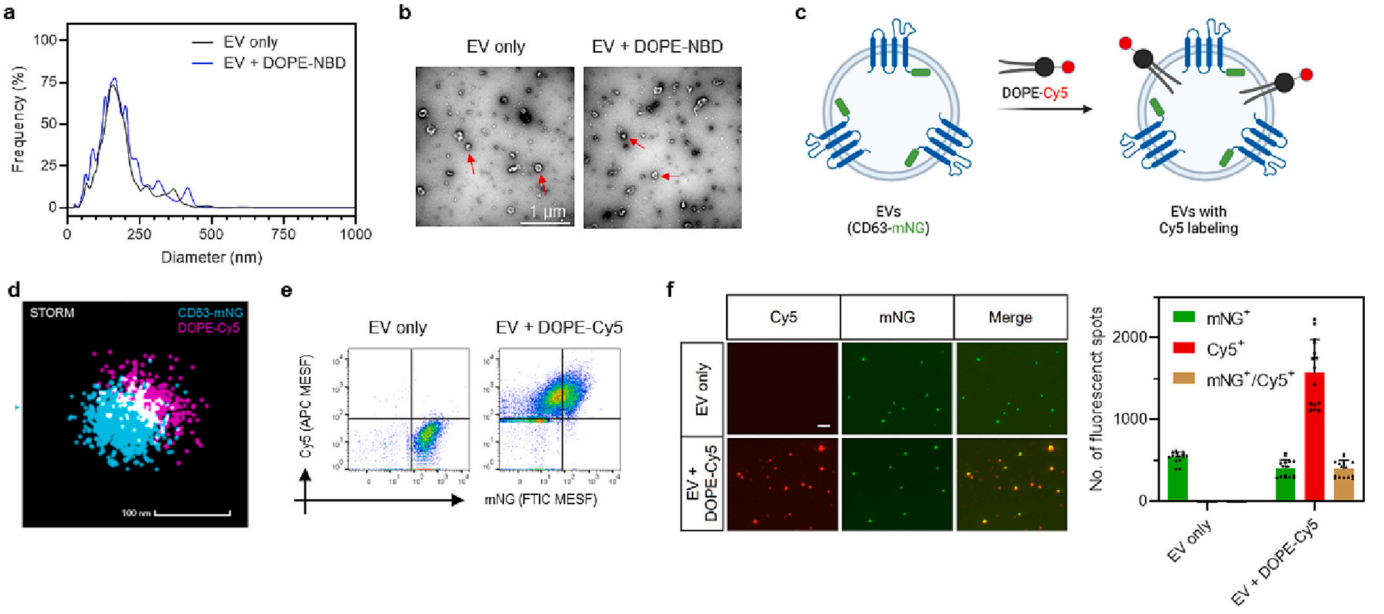

Fig. 4. EV engineering efficiency of DOPE in relative to genetical engineering. EVs from FreeStyle 293-F cells stably expressing CD63-mNG were incubated with DOPE conjugates and purified. (a) Size distribution of EVs after incubation with DOPE-NBD. Data were shown as the mean of three biological replicates. (b) Morphology of EVs after incubation with DOPE-NBD. (c) Scheme of labeling EVs using DOPE-Cy5. (d) High-resolution fluorescence microscopy of EVs after incubation with DOPE-Cy5. (e) Representative dot plots of EVs after incubation with DOPE-Cy5. (f) Single vesicle imaging of EVs after incubation with DOPE-Cy5. Crops of representative images were shown.Total single (mNG^+ or $Cy5^+$) and double ($mNG^+/Cy5^+$) positive fluorescent spots were quantified from 10 to 15 fields of view using EVAnalyzer [19]. Results were shown as mean ± standard deviation.

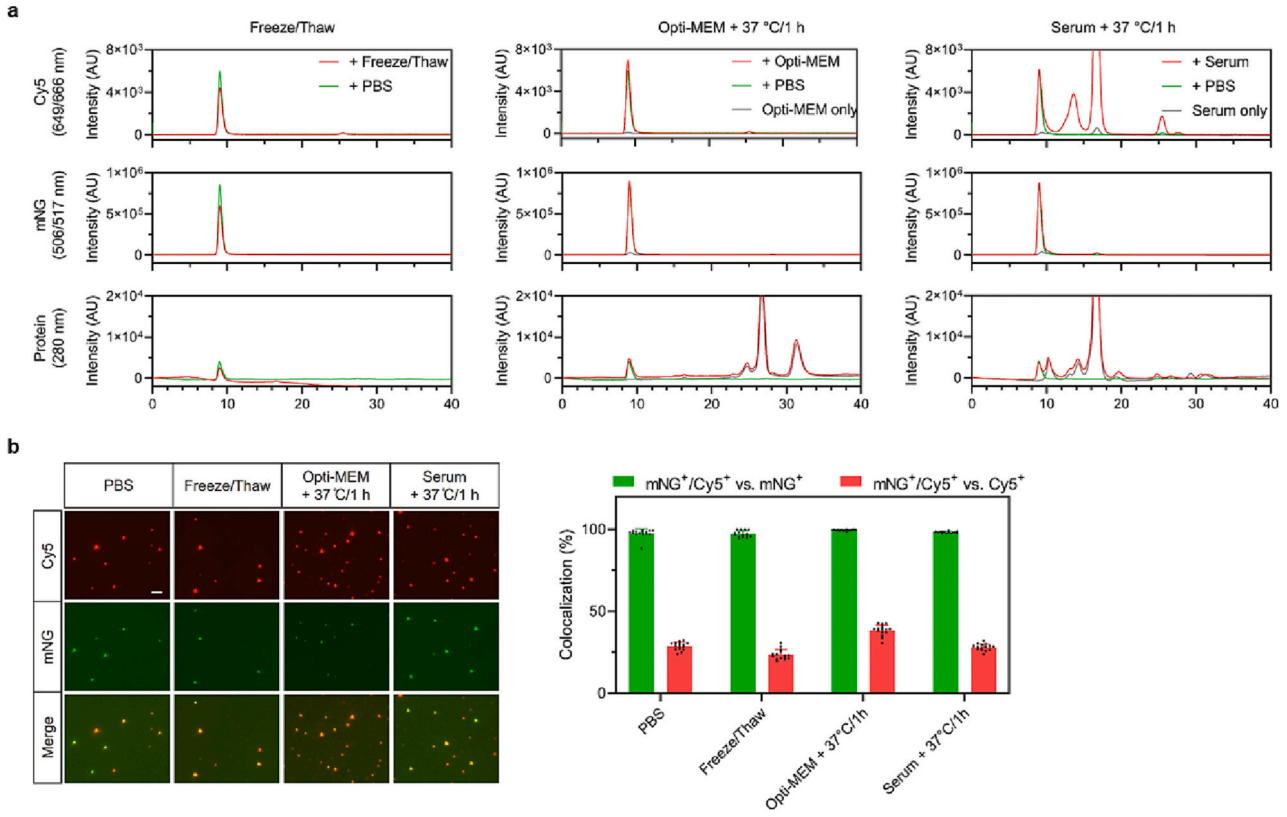

Fig. 5. Stability of DOPE-Cy5-engineered EVs. EVs from FreeStyle 293-F cells stably expressing CD63-mNG were incubated with DOPE-Cy5 and purified using qEV columns The labeled EVs were subjected to either a freeze/thaw cycle or incubated with Opti-MEM or serum for 1 h at 37 °C, and then analyzed by analytical SEC (a) followed by quantitative single vesicle imaging (b). Representative images and relative number of double positive ($mNG^+/Cy5^+$) spots *versus* total single positive spots (mNG^+ or $Cy5^+$) were shown. Results were shown as mean ± standard deviation.

(8.5–9.5 min, Fig. S5a), thus emergence of extra Cy5 peaks is indicative of DOPE dissociation from engineered EVs and/or re-distribution to other lipid-appealing components.

Neither freeze/thaw cycles nor incubation with Opti-MEM induced DOPE dissociation from engineered EVs because no additional Cy5 peaks were observed (Fig. 5a). Consistently, both the relative EV peak area in the Cy5 and mNG fluorescence channels remained constant (Fig. S5b). Noteworthy, incubating engineered EVs with mouse serum resulted in several additional Cy5 fluorescent peaks cofractionating with serum proteins, indicating DOPE dissociation and/or re-distribution. Interestingly, Cy5 fluorescence signals in the EV peak were unchanged, whereas Cy5 absorbance showed loss of signals (Fig. S5c). This indicates that Cy5 fluorescence is partially quenched upon tight packing onto vesicles, and a loss of molecules does not result into significant reduction of fluorescent brightness albeit detectable in the absorbance.

For the reason above, EVs isolated by size exclusion were additionally collected and analyzed by quantitative single vesicle analysis using the EVAnalyzer FijI plugin [19]. Analysis reveals that a majority of mNG^+ EVs (>95%) remained labeled by DOPE-Cy5 and that the fraction of double positive EVs in either mNG^+ or $Cy5^+$ EVs was not reduced by any of the treatments (Fig. 5b). Consistent with the chromatography data, the fluorescence brightness of the vesicles remained similar at all conditions despite a slight decline in Cy5 brightness after incubation in serum (Fig. S5d). Based on these data, we conclude that DOPE strongly associates with EVs withstanding standard storage conditions. In presence of serum, the label partially redistributes to serum components, whereas the number of labeled EVs and their fluorescence brightness is not significantly reduced due to saturation of fluorescence at high labeling stoichiometry.

2.6. Fluorescent DOPE conjugates enable tracking cellular uptake of engineered EVs

Despite the destabilizing effect of serum on DOPE-engineered EVs, the fact that cell culture media usually contains 10% serum inspires us to examine the feasibility of DOPE-based engineering in tracking cellular uptake of EVs. Results above showed that increasing DOPE concentration up to 3e5 molecules per EV would yield brighter EVs that are presumably beneficial for downstream visualization. Therefore, we purified engineered EVs that were prepared at varying DOPE-Cy5 concentrations and tracked their uptake dynamics in Huh-7 hepatoma cells using automated microscopy (Fig. 6a). At a labeling concentration as low as 6e3 DOPE molecules per EV, we observed significant time-dependent increases in cellular Cy5 signals (Fig. 6b). Higher labeling concentration of DOPE increased Cy5 intensity in recipient cells, but somehow led to noticable declines in cellular mNG signals.

Importantly, at a labeling concentration of 3e4 DOPE molecules per EV, the measurements of uptake dynamics of DOPE-EVs according to number of Cy5 and mNG spots per cell area were linearly correlated (Fig. 6c). Lowering EV dose in the treatment (from 5e10 till 5e9 per mL) further improved the correlation (Fig. S6), likely due to less saturation of Huh-7 cells at later treatment time points. Furthermore, mNG and Cy5 demonstrated a high degree of colocalization in recipient cells (Fig. 6a, Fig. 6d), implying similar fates of DOPE and mNG following internalization. Overall, the high correlation in uptake dynamics and colocalization in recipient cells imply that DOPE-based labeling is feasible to inform cellular uptake of EVs, but it's advised to optimize the labeling concentration of DOPE conjugates, treatment dose and duration.

2.7. Receptor-binding DOPE conjugates increase cellular uptake of engineered EVs

Besides fluorophores, DOPE can be conjugated to other moieties to impart novel properties to EVs. Increasing the uptake of EVs by target cells can boost their therapeutic efficacy. To explore whether DOPE-based engineering could be used to improve cellular uptake, targeting peptides with azide groups (Fig. S7a) were conjugated to DOPE-DBCO through the CLICK chemistry and appended to mNG-labeled EVs. In the first example, DOPE was conjugated with a chimeric peptide containing a RVG fragment that recognizes the acetylcholine receptor

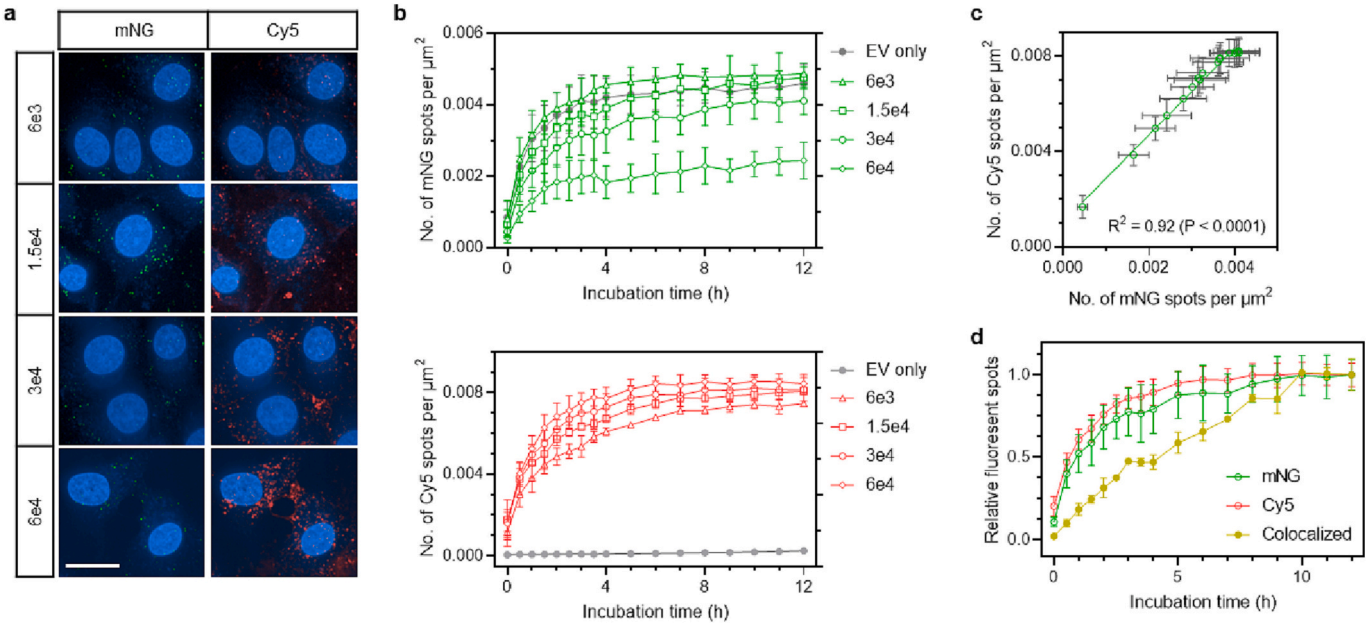

Fig. 6. Cellular uptake of DOPE-engineered EVs. (a) Representative microscope images of Huh-7 cells at 2 h after EV treatment. CD63-mNG EVs were incubated with varying concentrations of DOPE-Cy5 molecules per EV, purified to remove free lipid conjugates, and added to Huh-7 cells. Scale bar equals 25 μm. (b) Uptake dynamics of DOPE-engineered EVs as measured by Cy5 and mNG spots per μm^2 cell area. EVs were added to cells at 5e10/mL. (c) Correlation between the number of Cy5 and mNG spots per μm^2 cell area. CD63-mNG EVs were labeled with 3e4 DOPE-Cy5 molecules per EV and added to cells at 5e10/mL. Each dot indicates one time point. (d) Uptake dynamics of DOPE-engineered EVs as measured by single (mNG or Cy5) and double (mNG and Cy5, colocalized) fluorescent spots. Labeling concentration of DOPE-Cy5 was 3e4 molecules per EV and EVs were added to cells at 5e9/mL. Results were normalized to the maximal values. In (b-d), data were shown as the mean ± standard deviation of three biological replicates.

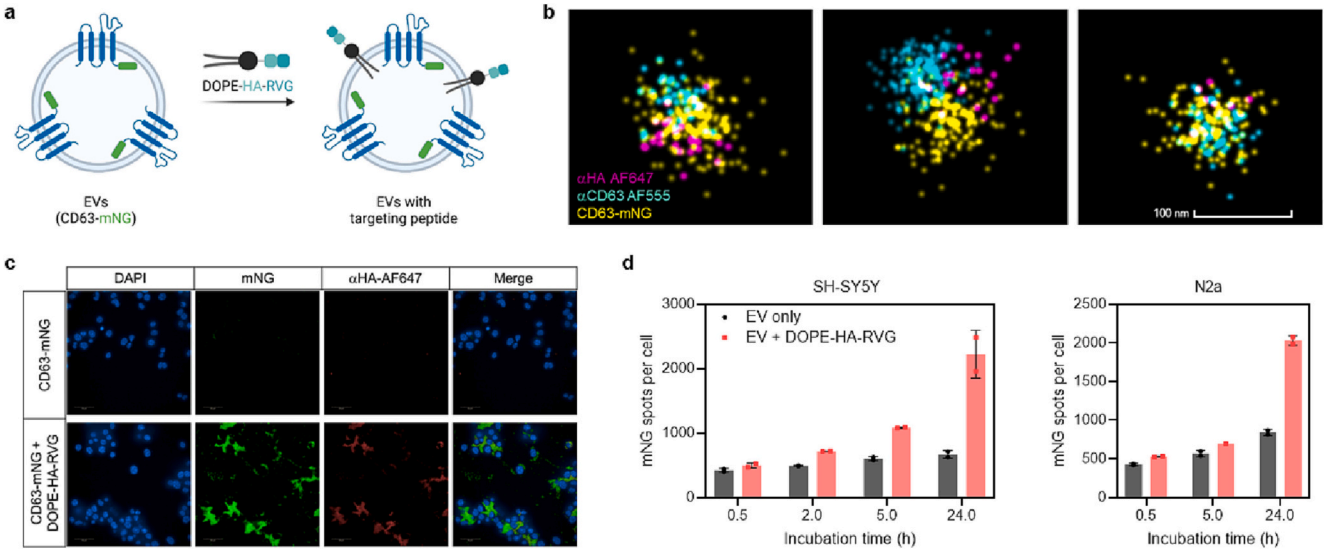

Fig. 7. Cellular uptake of DOPE-engineered EVs by neuroblastoma cells. (a) Scheme of preparation of acetylcholine receptor-binding EVs. CD63-mNG EVs were incubated with DOPE-HA-RVG (3e4 molecules per EV) and purified. (b) High-resolution fluorescence microscopy of CD63-mNG EVs after incubation with DOPE-HA-RVG and counter-staining with CD63 and HA. (c) Representative microscope images of SH-SY5Y cells 24 h after EV treatment. Scale bar equals 50 μm. (d) Uptake dynamics of DOPE-engineered EVs in SH-SY5Y and N2a cells as measured by mNG signals. In (c-d), EVs were added to cells at 1e11/mL. Data were shown as the mean ± standard deviation of two biological replicates.

(AChR) on neural cells [21,22] and an HA tag for immunofluorescence detection. Afterwards, CD63-mNG EVs were incubated with DOPE-HA-RVG conjugates and purified prior to analysis (Fig. 7a). DOPE-engineered EVs showed similar size distribution to pristine EVs (Fig. S7b). After counter-staining HA tag with AF647-conjugated antibody and CD63 with AF555-conjugated antibody, we observed spatial proximity between DOPE conjugates and EVs using super-resolution microscopy (Fig. 7b), confirming successful engineering.

Next, we examined the uptake of engineered EVs in two AChR-expressing cell lines, SH-SY5Y and N2a. In line with our assumption, clear increases in cellular mNG and AF647 intensity were observed (Fig. 7c). Quantification of mNG spots per cell at different time points corroborates the targeting ability of engineered EVs (Fig. 7d). Additionally, we conjugated bombesin, a 10-mer peptide ligand of the gastrin-releasing peptide-preferring receptor (GRPR) [23], with DOPE and tested its effect on cellular uptake of engineered EVs. Again, higher mNG intensity was observed in T47D cells that express the receptor (Fig. S7c). In conclusion, DOPE conjugates with targeting peptides could be used to engineer and improve cellular uptake of EVs *in vitro*.

2.8. *Albumin-binding DOPE conjugates increase plasma retention of engineered EVs*

Short half-life of EVs in plasma after intravenous administration greatly limits future therapeutic applications *in vivo*. Camouflaging biotherapeutics with serum albumin is a classic way for extending their

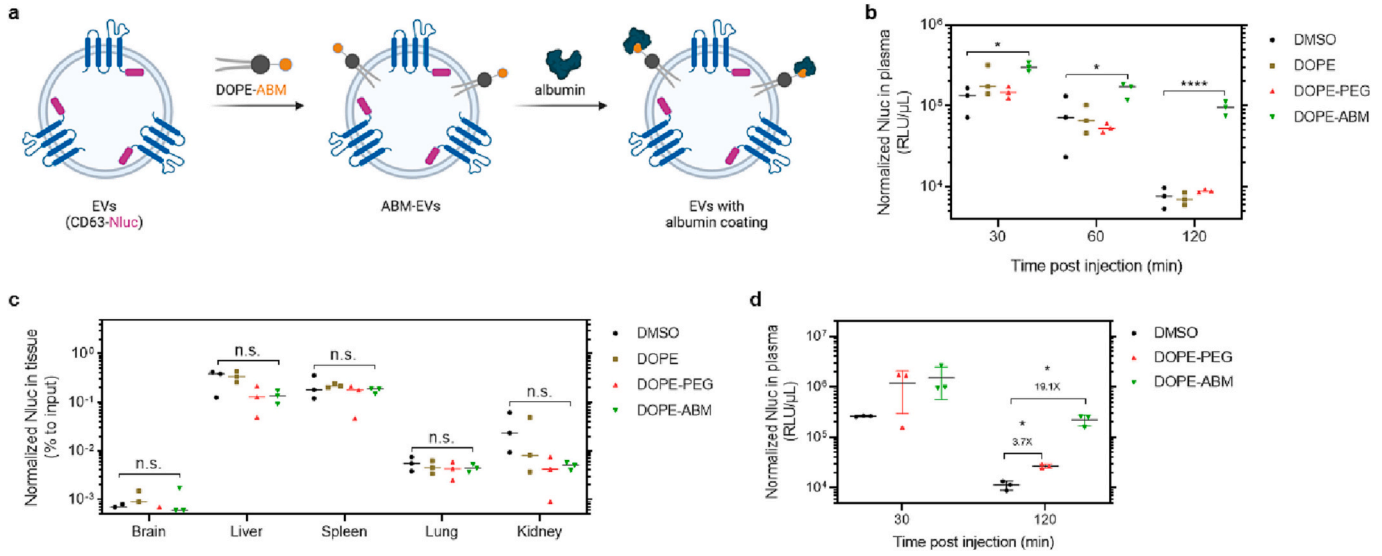

Fig. 8. Kinetics and distribution of DOPE-engineered EVs in mice. (a) Scheme of preparation of albumin-binding EVs. CD63-Nluc EVs were incubated with albumin-binding DOPE conjugates. (b) Level of CD63-Nluc EVs at different time point after intravenous injection. (c) Level of CD63-Nluc EVs in different tissues at 120 min after intravenous injection. In (b-C), EVs were incubated with 3e4 DOPE-ABM molecules per EV. (d) Level of CD63-Nluc EVs at different time point after intravenous injection. EVs were incubated with 6e4 DOPE-ABM molecules per EV. Data were shown as the mean ± standard deviation of three mice. Two-tailed unpaired *t*-test. n.s.: non-significant; *: $p < 0.05$; ****: $p < 0.0001$.

circulation time [24]. As such, we attached an albumin-binding molecule (ABM) to DOPE (Fig. S8a) [25] and tested if engineering EVs with DOPE-ABM extends the circulation time of EVs *in vivo*.

To facilitate quantification of engineered EVs *in vivo*, EVs were collected from FreeStyle 293-F cells stably expressing Nluc protein fused to CD63 and incubated with DOPE-ABM conjugates (Fig. 8a). Since the readout would be based on luminescence and there is overwhelming albumin *in vivo*, no purification step was used after engineering with DOPE-ABM. PEGylation is commonly used for improving the retention of synthetic nanoparticles in plasma but had little effect on EVs (Fig. 8b). In contrast, engineering with DOPE-ABM (3e4 molecules per EV) significantly increased EVs level in plasma at different time points, reaching around 12-fold increase 120 min after administration. Similar to EVs without exogenous engineering, most DOPE-ABM-engineered EVs accumulated in liver and spleen (Fig. S8b). No significant changes in terms of distribution to major organs at the endpoint were observed (Fig. 8c). Doubling the labeling concentration of DOPE-ABM conjugates from 3e4 to 6e4 molecules per EV further improved the fold change of EVs level in plasma (Fig. 8d). In conclusion, exogenous engineering of EVs with albumin-binding DOPE conjugates extends their retention in mouse plasma.

3. Discussion

In comparison with genetic engineering of EV producer cells and chemical engineering, physical association between molecules of interest and isolated EVs represents a simpler and more accessible strategy. The present study provides compelling results supporting the use of the phospholipid DOPE for direct labeling and functionalization of EVs. Specifically, our study relies on single vesicle flow cytometry for a direct comparison of different lipid anchors and highlights the superior efficiency of DOPE over other lipid anchors including ceramide [12], cholesterol [9,10], and DSPE [16–18]. Our comparison between DOPE and its analogs with different fatty acid chains underlines the importance of the hydrophobic tails. Looking at the structural differences of those phosphatidylethanolamines (Fig. 2), it appears that having the unsaturated fatty acid (oleoyl in the case of DOPE) could enhance the labeling efficiency while increasing the hydrophobicity (methyl in the case of DPhPE) enhances self-aggregation.

Of note, both the lipid anchor and the tag should be taken into consideration when engineering EVs with lipid conjugates. For instance, NBD-tagged ceramide exhibited rather poor labeling efficiency, but its BODIPY-tagged conjugates were much better (data not shown), suggesting a contributing or detrimental role of the fluorophore. Most importantly, we consistently found high engineering efficiency for all the DOPE conjugates in the study.

Despite the wide use of lipophilic dyes for exogenously labeling EVs, it is reportedly susceptible to dissociation which could lead to significant bias [26–28]. The lack of specificity of lipophilic dyes together with the subpopulation-limited nature of genetic engineering often result into diverging biodistribution patterns [28]. Herein, after incubating DOPE-engineered EVs with serum, we also observed dye dissociation and re-distribution to serum components (Fig. 5), calling for cautious consideration when applied in biodistribution studies. Interestingly, despite partial re-distribution of the dye, the number and brightness of the Cy5-DOPE labeled EVs remained almost unchanged, most likely due to saturation of fluorescence signals upon quenching at the high labeling densities used in our study.

Furthermore, in context of freeze/thaw cycles and cell culture studies where serum content was low ($\leq$ 10%), the limitation regarding dye re-distribution is barely a matter of concern. Specifically, we made a head-to-head comparison of genetic engineering and DOPE-based engineering by labeling CD63-mNG EVs with DOPE-Cy5 and correlating fluorescence intensity in both channels. Importantly, mNG and Cy5 signals were highly colocalized in recipient cells, and their dynamic changes approximated linear correlation. This is the first time, as far we know, to demonstrate that lipophilic dye-centered measurement is as reliable as reporter proteins genetically fused to EV-scaffold proteins, thereby providing an outstanding tool for labeling EVs that cannot be genetically engineered. Of similar importance, it is recommended to titrate the labeling concentration of DOPE because the excess, particularly more than 6e4 molecules per EV, negatively affected cellular mNG measurements. This trend might technically result from a quenching of mNG emission by Cy5 and/or altered lipid composition of EVs due to DOPE integration that hampers EVs uptake. If the second hypothesis is true, our results might imply an superior ability of EVs in the delivery of cargo molecules over liposomes and lipid nanoparticles that contain considerable amount of DOPE [29,30].

The ability of DOPE to anchor on the lipid bilayers of EVs provides ample opportunities for functionalization of EVs. Here, we showed that DOPE-based engineering can enable tracking internalization, increase cellular uptake, as well as enhance retention in mouse plasma of engineered EVs. Not only the moieties reported here (*i.e.*, fluorophore, targeting peptide, and albumin-binding molecule), but also pharmacological molecules like antigens and RNAs could be conjugated to DOPE and displayed on EV surface for therapeutic application in future.

4. Method

4.1. Cell culture

SH-SY5Y cells were maintained in MEM (Gibco, 11,095,080) and F12 (Gibco, 11,765,054) in ratio 1:1 supplemented with 10% fetal bovine serum (FBS; Gibco, 10,270–106), 5% sodium bicarbonate solution (Gibco, 25,080,094), 1% sodium pyruvate solution (Gibco, 11,360,039) and 1% non-essential amino acid solution (Gibco, 11,140,050). K562, Huh-7, N2a, and T47D cells were maintained in high glucose DMEM (Gibco, 41,966–029) supplemented with 10% FBS and 1% anti-anti (Gibco, 15,240). Freestyle 293-F cells were kept in FreeStyle 293-F Expression Media (Gibco, 12,338–018) under continuous shaking at 175 rpm. All cells were cultured in humidified incubators at 37 °C and 5% CO_2.

4.2. Synthesis of DOPE-Cy5

DOPE-DBCO (Merck, 870129C; 1 eq, 5 mg, 4.8 μmol) in 0.5 mL chloroform was added to Cy5-N_3 (Merck, 777,323; 1 eq, 5 mg, 4.8 μmol) in 0.3 mL DMSO. The reaction was slowly concentrated to half of the volume and continued for an additional 3 h. Two mL water was added to the mixture, and solvent was removed by freeze-drying to recover DOPE-Cy5 (compound **1**). Standard freeze-drying procedures included freezing samples in liquid nitrogen, freeze-drying overnight in HETO Freeze Drier with a collector at −120 °C, and vacuum below 10 mbar. After 18 h samples were visually dry. MS (M^2; UPLC-MS/MS Waters XEVO G2-S QTOF-MS) calculated = 930.25, found 930.45.

4.3. Synthesis of DOPE conjugates with peptides

HA-RVG peptides were synthesized by CASLO with C terminal azido lysine (Fig. S7a). To synthesize DOPE-HA-RVG, DOPE-DBCO (Merck, QBD10502; 1 eq, 0.5 mg, 0.048 μmol) in 0.05 mL chloroform was added to HA-RVG (1 eq, 0.3 mg, 0.048 μmol) in 0.05 mL dimethylformamide. After 3 h stirring, to reaction was added 2 mL water, and the product was recovered by freeze-drying. MS (M^-) calculated = 7399, found 7400.

BBN peptides with N-terminal azido were in-house synthesized with automated solid phase peptide synthesis (SPPS) using fluorenylmethyloxycarbonyl (Fmoc) strategy (Fig. S6). Rink Amide Chem Matrix (Biotage) resin was used to generate an amidated C-terminus. Automated SPPS was performed on an Alstra peptide synthesizer using five-fold molar excess of N-α-Fmoc-protected amino acids, ethyl 2-cyano-2-(hydroxyimino)acetate, and N,N′-diisopropylcarbodiimide

(DIC) in *N*-methylpyrrolidone (NMP). Fmoc protecting groups were cleaved using 20% piperidine in NMP (*v*/v). To synthesize DOPE-BBN, DOPE-DBCO (1 eq, 1.93 mg, 1.84 μmol) in 0.19 mL chloroform was added to BBN (1 eq, 2.3 mg, 1.84 μmol) in 0.19 mL DMSO. Reaction was slowly concentrated to half of the volume and allowed to continue for 3 h. Two mL water was added to the mixture, and the product was recovered by freeze-drying. MS (M^-) calculated = 2279.3, found 2279.3.

4.4. Synthesis of DOPE-PEG and DOPE-ABM

Azido-dPEG$_4$-acid (Merck, QBD10502; 2 eq, 0.24 mmol, 70 mg) was preactivated using HBTU (CAS No. 94790–37-1; 2 eq, 0.24 mmol, 91 mg) and NMM (CAS No. 109–02-4; 10 eq, 2.4 mmol, 242 mg, 263 μL) in 0.44 mL dimethylformamide at room temperature for 30 min. Then, ABM (synthesized according to the reference [25]; 1 eq, 0.12 mmol, 50 mg) and DIPEA (CAS No. 7087-68-5; 1 eq, 0.12 mmol, 15.5 mg, 208 μL) were dissolved in 0.4 mL dimethylformamide and added to the mixture, followed by gentle agitation at room temperature for 2 h. Compound **2** was purified using a reverse-phase HPLC system (Jasco) equipped with a UV detector (at 220 nm) and a Discovery BIO Wide Pore C18 column (Supelco; 5 μm, 25 cm × 21.2 mm). The mobile phase consisted of A (100 mM triethylammonium acetate, pH 7 containing 5% acetonitrile) and B (acetonitrile) with a gradient of 10–95% in 36 min at 5 mL/min. MS (M^{-1}) calculated = 690.20, found 690.19.

To synthesize DOPE-PEG (compound **3)**, Azido-dPEG$_4$-acid (1 eq, 2.4 μmol, 0.7 mg) and DOPE-DBCO (1 eq, 2.4 μmol, 2.5 mg) were dissolved in 0.25 mL chloroform. The mixture was gently agitated at room temperature for 3 h, and the solvent was removed by evaporation. MS (M^{-1}) calculated = 1720.77, found 1720.70. To synthesize DOPE-ABM (compound **4**), DOPE-DBCO (1 eq, 4.8 μmol, 5 mg) and compound **2** (1 eq, 4.8 μmol, 3.3 mg) were dissolved in 0.5 mL chloroform, followed by gentle agitation at room temperature for 3 h. The solvent was removed by evaporation. MS (M^{-1}) calculated = 1720.84, found 1720.84.

4.5. Generation of stable cell lines

Lentivirus vectors encoding the transgenes (CD63-mNG or CD63-Nluc) were produced using HEK-293 T as the packaging cells. Briefly, HEK-293 T were seeded in a T175 flask and cultured until confluency reaching around 60%. Then the cells were co-transfected with the expression plasmid, pCD/NL-BH (helper plasmid) and pcoPE01(envelope plasmid) overnight and cultured in complete DMEM supplemented with 10 mM sodium butyrate (Sigma-Aldrich, B5878) for 8 h. After culturing the cells in complete DMEM for an additional 22 h, conditioned media were filtered through 0.45 μm syringe filters and centrifuged at 25,000 *g* for 90 min at 4 °C. The pellets containing viral particles were resuspended with IMDM (Gibco, 12,440–053) supplemented with 20% FBS and stored at −80 °C. For transduction of FreeStyle 293-F, cells were seeded in Erlenmeyer flasks (Sigma-Aldrich, CLS431143) at 2.5e5/mL and cultured overnight before adding lentiviral vectors. Engineered cells were selected using 4 μg/mL puromycin (Sigma-Aldrich, P8833).

4.6. Isolation of extracellular vesicles

Conditioned media were centrifuged twice (700 *g* for 5 min and then 2000 g for 10 min) and filtered using 200 nm filters to sequentially deplete cells, cellular debris and large particles. The pre-cleared media were concentrated to roughly 80 mL using the tangential flow filtration system (TFF, Repligen, KrosFlo KR2i) equipped with 300 kDa cut-off hollow fiber filters (Spetrum Labs, D06-E300–05-N). Flow rate and transmembrane pressure were set at 100 mL/min and 3.0 psi, respectively. Further concentration of EVs was performed using 100 kDa cut-off spin-filter (Millipore, UFC910024) and stored in PBS containing human albumin and trehalose (HAT buffer) at −80 °C until use [31].

Cow milk-derived EVs were isolated as previously described [19,20]. Briefly, milk was defatted, and casein was removed by enzymatic coagulation. EVs were purified by TFF and covalently labeled with 10 μM of Cy7 (Lumiprobe, 2,408,482–09-5; 1e4 molecules per EV) for 1 h at 37 °C. Free dye was removed by TFF and labeled EVs were stored at 4 °C until further use.

4.7. Engineering extracellular vesicles with lipid conjugates

DMSO of cell culture grade was used to prepare stock and working solutions for all types of lipid conjugates. EVs were diluted with PBS to 1e10-1e12/mL depending on specific purposes and incubated with lipid conjugates (3e4 molecules per EV) at 37 C degree for 2 h if not otherwise specified. The amount of DMSO in the DOPE-EVs mixture was no higher than 5%. Besides the in-house synthesized DOPE conjugates, the following commercial lipid conjugates with NBD tags were tested: ceramide (ThermoFisher; D7540); cholesterol (Avanti; 810252P); DOPE (Avanti; 810145P); Lyso DOPE (Avanti; 810127C); DSPE (Avanti; 810141P); DPPE (Avanti; 810144P); DPhPE (Avanti; 810142P).

4.8. Purification of extracellular vesicles

EVs were purified using gravity-based size exclusion qEVcolumns (Izon, ICO-70; for small scale purification) or the automated size exclusion chromatography system (GE Healthcare Life Sciences, ÄKTA Start; for large scale purification). For the eluate of qEV columns, the first 3 mL were void volume and discarded, while the next 3 mL were enriched with EVs and collected according to the manufacturer's instructions. For Äkta system, EVs were seperated using a HiTrap Capto Core 700 column (GE Healthcare Life Sciences) and collected according to the absorbance from a 280 nm UV detector. Samples were further concentrated using 10 kDa cut-off spin-filters (Millipore, UFC901024) if necessary.

Analylytic size exclusion chromatography was performed on a Shimadzu custom-built system with a mobile phase degassing unit (Shimadzu DGU-20A3R), a PDA detector (Shimadzu SPD-M20A) and a fluorescence detector (Shimadzu RF-20A) with automated fraction collection (Shimadzu FRC-10A). The system was mounted in a cold cabinet to ensure constant temperature (4 °C) and the sample was eluted with isocratic elution at a flow of 0.8 mL/min in PBS on a dextran-agarose matrix column (Superdex® 200 Increase 10/300 GL, 30 cm × 10 mm, 8.6 μm). To test stability of EV labeling, CD63-mNG EVs pre-labeled with DOPE-Cy5 (2e10 particles/mL in PBS) were either subjected to a freeze/thaw cycle (−80 °C), incubated in Opti-MEM (EVs in PBS/Opti-MEM of 1/2) for 1 h at 37 °C, or incubated with serum from BL6/N mice (1:50) for 1 h at 37 °C. 50 μL of each sample was injected and elution was monitored by simultaneous detection of UV absorbance at 280 nm and 649 nm, as well as dual fluorescence detection at (ex/em: 506/517 nm for mNG; 649/666 nm for Cy5).

4.9. Nanoparticle tracking analysis

EVs were diluted in PBS if needed and measured for particle size and concentration using the Nanoparticle Tracking Analysis system (NTA; Malvern Panalytic, NanoSight NS500). Five videos (30-s each) were acquired for each sample with a screen gain of 10 and camera level of 13. Data were analyzed using NTA 3.2 software with a screen gain of 20 and a minimum track length of 3.

4.10. Western blotting

FreeStyle 293-F cells (1e6 cells) were lysed with RIPA buffer supplemented with protease inhibitors (Roche, 04693116001) and mixed with loading buffer. EVs (2e9 in 15 μL) were directly mixed with loading buffer (ThermoFisher, NP0007). The mixture were heated at 70 °C for 10 min and separated onto a NuPAGE Novex 4–12% Bis-Tris Protein Gel

(Invitrogen, NP0335BOX). Proteins were transferred to a nitrocellulose membrane (Invitrogen, IB23001) at 20 V for 7 min using the iBlot system. Membranes were passivated in blocking buffer (LI-COR, 927–60,004) at room temperature for 1 h under gentle shaking and incubated with primary antibody overnight at 4 °C. After rinsing with TBS supplemented with 0.1% Tween 20 (TBS-T) for three times, membranes were stained with secondary antibodies (1: 5000, LI-COR) for 1 h. After rinsing with TBS-T for three times and PBS once, membranes were imaged using Odyssey infrared imaging system (LI-COR, US). The following primary antibodies were used: anti-Calnexin (Abcam, ab22595; 1:1000), Syntenin-1 (Origene, TA504796; 1:1000) and TSG101 (Abcam, ab125011; 1:500).

4.11. Electron microscopy

Eight μL of EVs were added to Formvar/carbon-coated 400-mesh copper grids (Agar Scientific, 01814-F) and kept for 1 min. Extra liquid was absorbed using filter papers and the grids were rinsed with 8 μL distilled water for 1 min. The grids were then stained twice with 8 μL of 1% uranyl acetate for 1 min and rinsed with distilled water before air-drying for around 10 min. Transmission electron microscope images were acquired using a Tecnai 12 Spirit BioTwin microscope (FEI Company) at an accelerating voltage of 100 kV. Micrographs were recorded using a 2 K × 2 K Veleta CCD camera (Olympus Soft Imaging Solutions).

4.12. Fluorescence microscopy for extracellular vesicles

CD63-mNG EVs were incubated with DOPE-Cy5 and purified using the ÄKTA Start system as detailed above. For EVs engineered with DOPE-HA-RVG, samples were stained with antibodies for 2 h at room temperature followed by antibody removal with qEV. The following antibodies were used: anti-CD63-CF568 (ONI, 800–00005; 1:200) and anti-HA-AF647((ThermoFisher, 26,183-A647; 1:40). Fifty μL of purfied EVs were added to a polylysine-coated glass-bottom 18-well chamber (Ibidi, 81,817) and incubated overnight for EVs attachment. Samples were overlaid with ONI B-cubed buffer (ONI, 800–00002 and 800–00003) and imaged using Nanoimager (ONI). Widefield and super-resolution (dSTORM) images were processed using ImageJ and NimOS (ONI) software, respectively.

Alternatively, EVs after size exclusion were added onto 18 well μ-slides (Ibidi) or regular quartz glass slides and analyzed using the Olympus IX83 widefield fluorescence microscope with a 100× oil objective (UPLXAPO100XO NA1.45). A SPECX7IR-LFIB Light Engine (Lumencor) was used as excitation light source for the following wavelengths: 475/28 nm (mNG), 635/22 nm (Cy5) and 730/40 nm (Cy7). Either a Penta-Band dichroic mirror (AHF-SPX-PSEM) or specific emission filter cubes for the respective fluorophores were used in the optical path (49002-ET-EGFP filter cube: ET470/40× EX and ET525/50 m EM; 49,004-ET-CY3/TRITC filter cube: ET545/25× EX and ET605/70 m EM). For each condition, 10–15 fields of view were analyzed and quantified using the open-source ImageJ/FijI plugin EVAnalyzer [19].

4.13. Fluorescence microscopy for cells

Huh-7 cells were seeded in Cell Carrier Ultra 96-well plates (Perkin Elmer, 6,055,302) and incubated overnight. The cells were treated with purified EVs and stained with Hoechst 33342 (ThermoFisher, 62,249) for visualizing nuclei and CF405S Wheat Germ Agglutinin (Biotium, 29,027) for visualization of the cytoplasm. Time-lapse images were acquired using an automated high-throughput confocal microscope (Operetta CLS High content microscopy system, Perkin Elmer). Cell area was automatically defined based on Wheat Germ Agglutining staining of cytoplasm. The number of mNG-, Cy5-, and mNG/Cy5-positive spots per μm^2 cell area were quantified over time.

N2a and SH-SY5Y cells were grown in Cell Carrier Ultra 96-well plates and treated with purified EVs. Live cell imaging was performed after counter-staining with Hoechst 33342. The number of mNG-positive spots per cell was quantified over time. To check the subcellular location of engineered EVs, cells were fixed using formalin solution (Sigma, HT5012) for 10 min. Cells were rinsed with PBS and incubated with AF647 labeled anti-HA antibody (ThermoFisher, 26,183-A647; 1:200) diluted in PBS containing 5% BSA (Sigma, A2153) and 0.02% saponin (Sigma, 84,510). Cells were incubated for 1 h at room temperature and rinsed three times with PBS to remove excess antibodies. After counter-staining nuclei with DAPI (ThermoFisher, 62,248), cells were rinsed three times and imaged using Operetta CLS High content microscopy system.

T47D cells were seeded in polymer-bottom 24-well plates (Ibidi, cat. no. 82426) and incubate overnight. The cells were treated with purified EVs for 4 h. Nuclei were stained with Hoechst 33422 just before the live cell imaging. Confocal images were acquired on a Nikon C2+ confocal microscope equipped with a water-immersion 60× objective with numerical aperture 1.20 (Nikon Instruments). Image processing was performed by using FIJI. Background from images was manually removed by scaling the brightness and contrast.

4.14. Flow cytometry for extracellular vesicles

EVs engineered with fluorescent lipid conjugates were diluted in HAT buffer to 5e6/mL and measured from U-bottom 96-well plates using the Amnis® CellStream flow cytometer (Luminex). Data recording was triggered by any channel and lasted for 5 min at a sample flow rate of 3.44 μL/min. SSC and Cy5 signals were collected in channel 1 (773 ± 56 nm filter) and B6 (702 ± 87 nm filter), respectively. NBD and mNG signals were collected in channel C3 (528 ± 46 nm filter). Another flow cytometer, NanoAnalyzer (NanoFCM), was also used for detecting EVs at a single-vesicle level. Data recording was triggered by side scatter signals. SSC signals were collected in channel SPCM-1 (488 ± 10 nm filter). NBD signals were excited by the 488 laser and collected in channel SPCM-2 (528 ± 40 nm filter). All flow cytometry data were analyzed with optimized masking settings using the FlowJo software (v10.6.2).

4.15. Quantification of extracellular vesicles in mouse

Female Balb/c mice of around 20 g were bought from the Janiver Labs, and all procedures were performed per ethical permission granted by the Swedish Jordbruksverket (No. 13849–2020). Mice were injected with 100 μL of Nluc-labeled EVs (1e11 particles per mouse) through the tail vein. Blood samples were withdrawn from the tail vein 30 min, 60 min and 120 min after injection and placed in heparinized tubes. Major organs were collected after sacrificing the mice.

Blood samples were centrifuged at 2000 *g* for 10 min to retrieve plasma. The organs were weighed and lysed in 1 mL of 0.1% Triton X-100 solution (QIAGEN, TissueLyser II). Nluc activity in plasma and tissue lysate was measured as a surrogate of EVs. Specifically, 5 μL of plasma was mixed with 20 μL of 0.1% Triton X-100 solution in a white-walled 96-well plate, and the plate was shaken horizontally at 500 rpm for 5 min. A microplate luminometer (Promega, GloMax 96) was used to automatically inject the substrate Nano-Glo (Promega, N1130) at 25 μL per well and measure luminescence intensity. Tissue lysate was first diluted by 10-fold before adding the Nluc substrate.

4.16. Data analysis

Statistical analysis and graph plotting were performed using the GraphPad Prism software (v9). Results were shown as mean ± standard deviation of biological replicates and analyzed using two-tailed unpaired *t*-test. n.s.: non-significant; *: $p < 0.05$; ****: $p < 0.0001$.

Author contribution

Malgorzata Honcharenko and Samir EL-Andaloussi conceived the

project. Stability and single vesicle imaging experiments were performed by Melanie Schürz under supervision by Nicole Meisner-Kober. Wenyi Zheng, Malgorzata Honcharenko, Rim Jawad Wiklander, Oskar Gustafsson, Dhanu Gupta, Antonella Barone, Radka Slovak, Andrei Traista, Daria Farcas, Eleni Kyriakopoulou, Valentina Galli, Arianna Coluzzi, Heena Sharma, Samantha Roudi designed and performed all other experiments. Wenyi Zheng wrote the manuscript. All authors discussed the results and edited the manuscript.

Declaration of Competing Interest

SEA are consultants for and have equity interests in EVOX Therapeutics Ltd., Oxford, UK. The other authors declare no competing interests.

Data availability

All data supporting this project are available in the manuscript and supplementary material.

Acknowledgment

The study was supported by the Live Cell Imaging unit/Nikon Center of Excellence, BioNut. S.E.-A. is supported by H2020 (EXPERT), the Swedish foundation of Strategic Research (FormulaEx, SM19-0007), ERC CoG (DELIVER) and the Swedish Research Council (4–258/2021).

Appendix A. Supplementary data

Supplementary data to this article can be found online at https://doi.org/10.1016/j.jconrel.2023.04.033.

References

[1] G. van Niel, et al., Challenges and directions in studying cell–cell communication by extracellular vesicles, Nat. Rev. Mol. Cell Biol. 23 (2022) 369–382.
[2] D. Gupta, et al., Amelioration of systemic inflammation via the display of two different decoy protein receptors on extracellular vesicles, Nat. Biomed. Eng. 5 (2021) 1084–1098.
[3] O.P.B. Wiklander, M. Brennan, J. Lötvall, X.O. Breakefield, S.E.L. Andaloussi, Advances in therapeutic applications of extracellular vesicles, Sci. Transl. Med. 11 (2019) 1–16.
[4] M. Richter, P. Vader, G. Fuhrmann, Approaches to surface engineering of extracellular vesicles, Adv. Drug Deliv. Rev. 173 (2021) 416–426.
[5] S. Kwon, et al., Engineering approaches for effective therapeutic applications based on extracellular vesicles, J. Control. Release 330 (2021) 15–30.
[6] X. Jia, J. Tang, C. Yao, D. Yang, Recent Progress of extracellular vesicle engineering, ACS Biomater. Sci. Eng. 7 (2021) 4430–4438.
[7] S.A.A. Kooijmans, J.J.J.M. Gitz-Francois, R.M. Schiffelers, P. Vader, Recombinant phosphatidylserine-binding nanobodies for targeting of extracellular vesicles to tumor cells: a plug-and-play approach, Nanoscale 10 (2018) 2413–2426.
[8] S.A.A.A. Kooijmans, et al., Electroporation-induced siRNA precipitation obscures the efficiency of siRNA loading into extracellular vesicles, J. Control. Release 172 (2013) 229–238.
[9] M.-C. Didiot, et al., Exosome-mediated delivery of Hydrophobically modified siRNA for huntingtin mRNA silencing, Mol. Ther. 24 (2016) 1836–1847.
[10] A.J. O'Loughlin, et al., Functional delivery of lipid-conjugated siRNA by extracellular vesicles, Mol. Ther. 25 (2017) 1580–1587.
[11] G. Cui, et al., RVG-modified exosomes derived from mesenchymal stem cells rescue memory deficits by regulating inflammatory responses in a mouse model of Alzheimer's disease, Immun. Ageing 16 (2019) 10.
[12] T. Tertel, et al., Imaging flow cytometry challenges the usefulness of classically used extracellular vesicle labeling dyes and qualifies the novel dye exoria for the labeling of mesenchymal stromal cell–extracellular vesicle preparations, Cytotherapy 24 (2022) 619–628.
[13] F. Abel, et al., Extracellular vesicles isolated from patients undergoing remote ischemic preconditioning decrease hypoxia-evoked apoptosis of cardiomyoblasts after isoflurane but not propofol exposure, PLoS One 15 (2020), e0228948.
[14] A.T. Boysen, et al., Fluorescent labeling of helminth extracellular vesicles using an in vivo whole organism approach, Biomedicines 8 (2020).
[15] A. Görgens, et al., Optimisation of imaging flow cytometry for the analysis of single extracellular vesicles by using fluorescence-tagged vesicles as biological reference material, J. Extracell. Vesicl. 8 (2019) 1587567.
[16] K. Feng, et al., Reversing the surface charge of MSC-derived small extracellular vesicles by εPL-PEG-DSPE for enhanced osteoarthritis treatment, J. Extracell. Vesicl. 10 (2021), e12160.
[17] Y. Cao, et al., Engineered exosome-mediated near-infrared-II region V 2 C quantum dot delivery for nucleus-target low-temperature Photothermal therapy, ACS Nano 13 (2019) acsnano.8b07224.
[18] Z. Wang, et al., Exosomes decorated with a recombinant SARS-CoV-2 receptor-binding domain as an inhalable COVID-19 vaccine, Nat. Biomed. Eng. 6 (2022) 791–805.
[19] M. Schürz, et al., EVAnalyzer: high content imaging for rigorous characterisation of single extracellular vesicles using standard laboratory equipment and a new open-source ImageJ/Fiji plugin, J. Extracell. Vesicl. 11 (2022) 12282.
[20] Nicole Meisner-Kober, Marteen De Groot, Martin Hintersteiner-Wenzel, R. Manzotti, Extracellular Vesicles From Milk and Process for Isolating the Same, 2021.
[21] L. Alvarez-Erviti, et al., Delivery of siRNA to the mouse brain by systemic injection of targeted exosomes, Nat. Biotechnol. 29 (2011) 341–345.
[22] P. Kumar, et al., Transvascular delivery of small interfering RNA to the central nervous system, Nature 448 (2007) 39–43.
[23] A.A. Begum, P.M. Moyle, I. Toth, Investigation of bombesin peptide as a targeting ligand for the gastrin releasing peptide (GRP) receptor, Bioorg. Med. Chem. 24 (2016) 5834–5841.
[24] X. Liang, et al., Extracellular vesicles engineered to bind albumin demonstrate extended circulation time and lymph node accumulation in mouse models, J. Extracell. Vesicl. 11 (2022), e12248.
[25] S. Trüssel, et al., New strategy for the extension of the serum half-life of antibody fragments, Bioconjug. Chem. 20 (2009) 2286–2292.
[26] S.T.-Y. Chuo, J.C.-Y. Chien, C.P.-K. Lai, Imaging extracellular vesicles: current and emerging methods, J. Biomed. Sci. 25 (2018) 91.
[27] P. Gangadaran, C.M. Hong, B.-C. Ahn, An update on in vivo imaging of extracellular vesicles as drug delivery vehicles, Front. Pharmacol. 9 (2018).
[28] E. Lázaro-Ibáñez, et al., Selection of fluorescent, bioluminescent, and radioactive tracers to accurately reflect extracellular vesicle biodistribution in vivo, ACS Nano 15 (2021) 3212–3227.
[29] Y. Hattori, S. Suzuki, S. Kawakami, F. Yamashita, M. Hashida, The role of dioleoylphosphatidylethanolamine (DOPE) in targeted gene delivery with mannosylated cationic liposomes via intravenous route, J. Control. Release 108 (2005) 484–495.
[30] X. Hou, T. Zaks, R. Langer, Y. Dong, Lipid nanoparticles for mRNA delivery, Nat. Rev. Mater. 6 (2021) 1078–1094.
[31] A. Görgens, et al., Identification of storage conditions stabilizing extracellular vesicles preparations, J. Extracell. Vesicl. 11 (2022), e12238.